Athermal silicon waveguides with bridged subwavelength gratings for TE and TM polarizations

Marc Ibrahim,^{1,*} Jens H. Schmid,² Alireza Aleali¹, Pavel Cheben,² Jean Lapointe,² Siegfried Janz,² Przemek J. Bock,² Adam Densmore,² Boris Lamontagne,² Rubin Ma,² Dan-Xia Xu,² and Winnie N. Ye¹

¹Department of Electronics, Carleton University, 1125 Colonel By Drive Ottawa, Ontario, Canada ²Institute for Microstructural Sciences (IMS), National Research Council Canada (NRC), 1200 Montreal Road, Ottawa, Ontario, Canada *mibrahi3@doe.carleton.ca

Abstract: In this paper, athermal silicon waveguides using bridged subwavelength grating (BSWG) structures are proposed and investigated. The realization of temperature-independent BSWG waveguides for both polarizations is demonstrated numerically and experimentally. SU-8 polymer is used as the cladding material to compensate for the positive thermo-optic (TO) coefficient (dn/dT) of silicon. We investigate the dependence of the effective TO coefficient of BSWG waveguides on both the bridge width and grating duty cycle. The BSWG waveguides have a width of 490 nm, a height of 260 nm, and a grating pitch of 250 nm. Athermal behavior is achieved for both the transverse-magnetic (TM) and the transverse-electric (TE) polarized light for a variety of bridge width and duty cycle combinations. Furthermore, the BSWGs can be designed to be athermal for both TE and TM polarization simultaneously.

©2012 Optical Society of America

OCIS codes: (230.0230) Optical devices; (060.4510) Optical communications; (230.7370) Waveguides; (250.5460) Polymer waveguides; (050.6624) Subwavelength structures.

References and links

- P. J. Bock, P. Cheben, J. H. Schmid, J. Lapointe, A. Delâge, S. Janz, G. C. Aers, D.-X. Xu, A. Densmore, and T. J. Hall, "Subwavelength grating periodic structures in silicon-on-insulator: a new type of microphotonic waveguide," Opt. Express 18(19), 20251–20262 (2010).
- P. Cheben, P. J. Bock, J. H. Schmid, J. Lapointe, S. Janz, D.-X. Xu, A. Densmore, A. Delâge, B. Lamontagne, and T. J. Hall, "Refractive index engineering with subwavelength gratings implemented in a highly efficient microphotonic coupler and a planar waveguide multiplexers," Opt. Lett. 35, 2526–2528 (2010).
- 3. C. F. R. Mateus, M. C. Y. Huang, L. Chen, C. J. Chang-Hasnain, and Y. Suzuki, "Broad-band mirror (1.12-1.62 um) using a subwavelength grating," IEEE Photon. Technol. Lett. **16**(7), 1676–1678 (2004).
- 4. J. H. Schmid, P. Cheben, S. Janz, J. Lapointe, E. Post, and D.-X. Xu, "Gradient-index antireflective subwavelength structures for planar waveguide facets," Opt. Lett. **32**(13), 1794–1796 (2007).
- P. Cheben, D.-X. Xu, S. Janz, and A. Densmore, "Subwavelength waveguide grating for mode conversion and light coupling in integrated optics," Opt. Express 14(11), 4695–4702 (2006).
- R. Halir, P. Cheben, J. H. Schmid, R. Ma, D. Bedard, S. Janz, D.-X. Xu, A. Densmore, J. Lapointe, and I. Molina-Fernández, "Continuously apodized fiber-to-chip surface grating coupler with refractive index engineered subwavelength structure," Opt. Lett. 35(19), 3243–3245 (2010).
- U. Levy, M. Abashin, K. Ikeda, A. Krishnamoorthy, J. Cunningham, and Y. Fainman, "Inhomogenous dielectric metamaterials with space-variant polarizability," Phys. Rev. Lett. 98(24), 243901 (2007).
- I. Glesk, P. J. Bock, P. Cheben, J. H. Schmid, J. Lapointe, and S. Janz, "All-optical switching using nonlinear subwavelength Mach-Zehnder on silicon," Opt. Express 19(15), 14031–14039 (2011).
- M. Ibrahim, J. H. Schmid, P. Cheben, J. Lapointe, S. Janz, P. J. Bock, A. Densmore, B. Lamontagne, R. Ma, D.-X. Xu, and W. N. Ye, "Athermal silicon subwavelength grating waveguides," Proc. SPIE 8707, 80071L (2011).
- J. H. Schmid, P. Cheben, S. Janz, J. Lapointe, E. Post, A. Delâge, A. Densmore, B. Lamontagne, P. Waldron, and D.-X. Xu, "Subwavelength grating structures in silicon-on-insulator waveguides," Adv. Opt. Technol. 2008, 685489 (2008).

- J. H. Schmid, P. J. Bock, P. Cheben, W. Sinclair, J. Garcia, S. Janz, J. Lapointe, G. C. Aers, D. Poitras, Y. Li, G. Lopinski, A. Delâge, A. Densmore, B. Lamontagne, R. Ma, and D.-X. Xu, "Applications of subwavelength grating structures in silicon-on-insulator waveguides," Proc. SPIE **7606**, 76060F (2010).
- W. N. Ye, J. Michel, and L. C. Kimerling, "Athermal high-index-contrast waveguide design," IEEE Photon. Technol. Lett. 20(11), 885–887 (2008).
- J. H. Schmid, M. Ibrahim, P. Cheben, J. Lapointe, S. Janz, P. J. Bock, A. Densmore, B. Lamontagne, R. Ma, W. N. Ye, and D.-X. Xu, "Temperature-independent silicon subwavelength grating waveguides," Opt. Lett. 36(11), 2110–2112 (2011).
- S. G. Johnson, "The MIT Photonic-Bands Manual (MPB)", Massachusetts Institute of Technology (MIT), http://ab-initio.mit.edu/mpb/doc/mpb.pdf
- G. Ghosh, "Model for the thermo-optic coefficients of some standard optical glasses," J. Non-Cryst. Solids 189(1-2), 191–196 (1995).
- D.-X. Xu, A. Densmore, A. Delâge, P. Waldron, R. McKinnon, S. Janz, J. Lapointe, G. Lopinski, T. Mischki, E. Post, P. Cheben, and J. H. Schmid, "Folded cavity SOI microring sensors for high sensitivity and real time measurement of biomolecular binding," Opt. Express 16(19), 15137–15148 (2008).
- J. H. Schmid, W. Sinclair, J. García, S. Janz, J. Lapointe, D. Poitras, Y. Li, T. Mischki, G. Lopinski, P. Cheben, A. Delâge, A. Densmore, P. Waldron, and D.-X. Xu, "Silicon-on-insulator guided mode resonant grating for evanescent field molecular sensing," Opt. Express 17(20), 18371–18380 (2009).

1. Introduction

Subwavelength grating waveguides (SWGs) have been proven to be an interesting alternative to conventional photonic wire (PW) waveguides [1]. The SWG is a new type of microphotonic waveguide which provides an extra degree of freedom in the design of photonic circuits since the refractive index of the waveguide core can be controlled by changing the grating duty cycle [1, 2]. The SWG waveguide structure is shown schematically in Fig. 1(a), where the duty cycle (DC) is defined as a/Λ . In order to suppress diffraction effects, the grating period is chosen smaller than half of the operating wavelength of light inside the medium. In such case, photonic bandgap opening is avoided and light propagation through the periodic structure resembles that in a homogeneous effective medium.

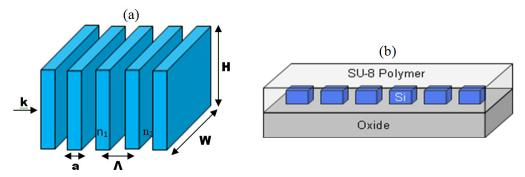


Fig. 1. a) Schematic of a subwavelength grating (SWG) waveguide core: *W* is the waveguide width, *H* is the waveguide height, *a* is the length of a silicon core segment, Λ is the grating pitch (period), *k* is the wavevector, and n₁ and n₂ are the core and cladding indices, respectively. b) Schematic of an athermal SWG waveguide.

Subwavelength high-index contrast gratings were first proposed as high-reflectivity mirrors [3], antireflective layers [4], fiber-chip couplers [2, 5, 6], lenses [7], terahertz optical switches [8] and more recently also as athermal waveguides [9–12]. The latter (shown in Fig. 1(b)) are technologically important because the strong temperature dependence of conventional silicon waveguides imposes stringent temperature control requirements for practical applications. The realization of temperature-independent waveguides, i.e. with an effective thermo-optic coefficient $dn_{eff}/dT \approx 0$, has been made possible by combining two materials with opposite thermo-optic (TO) coefficients [12, 13]. This was achieved for the first time in conventional strip waveguide geometry [12] and recently also in an SWG waveguide [13]. SU-8 polymer was used as the cladding material [13] since its negative TO coefficient ($dn/dT \approx -1.1 \times 10^{-4} \text{ K}^{-1}$) can compensate for the positive TO coefficient of silicon

 $(1.9 \times 10^{-4} \text{ K}^{-1})$. Athermal operation was achieved by changing the waveguide width and the SWG duty cycle to vary the effective mode overlap with the Si and SU-8 materials [13].

Simulations and measurements of the effective TO coefficient of different SWG waveguide configurations have been reported in [9] and [13]. The effective waveguide TO coefficient was estimated by measuring the spectral transmittance of unbalanced Mach-Zehnder interferometers with arms comprising SWG waveguides of varying duty cycles, at different temperatures. In the MZIs, conventional photonic wire (PW) waveguides were used for Y splitters and waveguide bends, and high-efficiency mode transformers [2] were used to connect the PW waveguides with the SWG waveguides. Athermal behavior was achieved for various geometries either for TE or for TM polarization, as summarized in Table 1.

Waveguide Width (W) (nm)	Waveguide Height (H) (nm)	Grating Pitch (A) (nm)	Polarization	Duty Cycle (DC = a/Λ) (%)
350	260	300	TE TM	79 90
450	260	300	TE TM	61 83
70	260	250	TE TM	60 84

Table 1. Some SWG waveguide geometries yielding athermal operation

In practice, however, waveguides with such high grating duty cycles are difficult to realize in fabrication since impractically small gaps are required, particularly for TM polarization (~50 nm). In order to circumvent this problem, here we demonstrate a new athermal waveguide configuration, namely a bridged subwavelength grating (BSWG) waveguide.

In a BSWG waveguide, the silicon segments of a conventional SWG waveguide are "bridged" together with silicon segments of a narrower width, as it is schematically shown in Fig. 2(a). The SEM images of two fabricated BSWG waveguides are shown in Fig. 2(b) and 2(c).

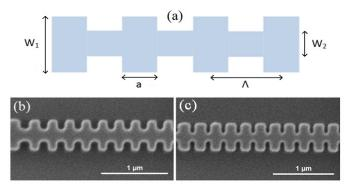


Fig. 2. (a) A schematic top view of the athermal BSWG waveguide. W_1 is the width of the wider silicon core segments, W_2 is the width of the bridging silicon segments, *a* is the length of the wider segments, and Λ is the grating pitch. The grating duty cycle (DC) is defined as a/Λ . (b, c) SEM images of fabricated BSWG waveguides. These waveguides were designed with $W_1 = 450$ nm, H = 260 nm, and $\Lambda = 250$ nm: (b) with DC = 50% and $W_2 = 140$ nm; (c) with DC = 65% and $W_2 = 80$ nm.

2. Simulations and design

We studied various waveguide geometries using the MIT Photonic Band (MPB) software [14], which numerically solves Maxwell's equations for periodic structures. The effective mode index (n_{eff}) of the BSWG waveguide is calculated for different temperatures, using the TO coefficients of silicon and SU-8. Since the TO coefficient of the buried oxide layer is

much smaller ($dn/dT = 9.33 \times 10^{-6} \text{ K}^{-1}$ for vitreous silica, or silica glass) compared to Si and SU-8, its effect is assumed to be negligible in our simulations [15].

The waveguide width, height, and grating pitch were 450 nm, 260 nm, and 250 nm, respectively. The required duty cycle for athermal condition at a wavelength of $\lambda = 1550$ nm is dependent on the light polarization and waveguide geometry. We first investigated the influence of the bridge width (W₂) and the duty cycle (DC) on the effective TO coefficient of the waveguide.

For a given DC, the athermal condition can be fulfilled by judiciously choosing the bridge widths W_2 . Nevertheless, the optimal value of W_2 is polarization dependent. For example, at a 35% duty cycle, the athermal condition requires bridge widths of 200 nm and 190 nm, for TE and TM polarizations, respectively. As the duty cycle increases, for example, to 50%, the athermal condition is achieved for $W_2 = 135$ nm (TE) and $W_2 = 160$ nm (TM).

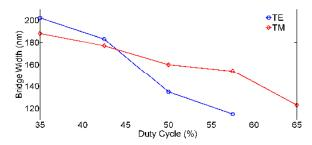


Fig. 3. The bridge width (W₂) dependence on the duty cycle (DC) in athermal BSWG waveguides with W₁ = 450 nm, H = 260 nm, and Λ = 250 nm. The operating wavelength is 1550 nm.

Figure 3 presents the bridge width (W_2) dependence on the grating duty cycle (DC) for athermal conditions in BSWG waveguides. It is observed that, unlike in the previously reported athermal SWG waveguides [13], temperature-independent operation can be achieved for either TE or TM polarizations with readily manufacturable minimum feature sizes. In addition, athermal behavior for both TE and TM polarizations is predicted for DC = 44% and W_2 = 175 nm. For this specific geometry, the mode effective indices as calculated by MPB are n_{TE} = 1.87 and n_{TM} = 1.77. This advantage of achieving a single athermal design for both TE and TM polarizations is a significant advance relevant for practical applications of silicon microphotonic devices.

3. Experimental results

The effective TO coefficient was measured using the methodology reported in [9]. An unbalanced Mach-Zehnder interferometers with arms comprising BSWG waveguides of varying duty cycles and bridge widths were manufactured by e-beam lithography, followed by reactive ion etching (RIE). The geometrical imbalance (length difference) between the two arms is $\Delta L = 3$ mm. For the Y splitters and waveguide bends, standard photonic wire (PW) waveguides are used, being connected with the SWG waveguides with high-efficiency mode transformers [2].

In Fig. 4, the transmission spectra for TM polarization are shown at different temperatures for a MZI device comprising photonic wire waveguides (Fig. 4(a)) and are compared with the spectra of a MZI with BSWG waveguides (Fig. 4(b)). It can be observed that the temperature-induced wavelength shift is substantially reduced for the BSWG device. Compared to a photonic wire waveguide with the measured TO coefficient $dn_{eff}/dT = 8.5 \times 10^{-5} \text{ K}^{-1}$, a near athermal operation with $dn_{eff}/dT = -6 \times 10^{-6} \text{ K}^{-1}$ was achieved for BSWG waveguides. The TO coefficient was calculated from the measured temperature induced wavelength shift as: $dn_{eff}/dT = (n_g/\lambda)(d\lambda/dT)$ [13, 16]. The group index n_g was calculated from the free spectral range $\Delta\lambda$ of the Mach-Zehnder interferometer: $n_g = \lambda^2/(\Delta\lambda\Delta L)$ [13, 17]. We were not able to

determine the numerical value of the waveguide propagation loss with sufficient accuracy from our data but it appears to be in the same range or slightly greater than the loss of PW and SWG waveguides, i.e. on the order of several dB/cm.

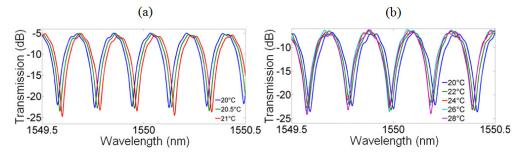


Fig. 4. The spectral transmittance of MZI with (a) photonic wire waveguides and (b) near athermal BSWGs. A wavelength shift $d\lambda/dT \approx 35 \text{ pm/}^{\circ}\text{C}$ is observed in (a). $d\lambda/dT \approx 2.5 \text{ pm/}^{\circ}\text{C}$ is observed in (b). Waveguide dimensions are: (a) W = 490 nm and H = 260 nm; (b) W₁ = 490 nm, H = 260 nm, $\Lambda = 250 \text{ nm}$, DC = 42%, and W₂ = 220 nm.

Measured wavelength dependence of the waveguide TO coefficient is shown in Fig. 5. It is observed that BSWG waveguides with a grating duty cycle of 58% are temperature independent for a bridge width of 140 nm, for TM polarization. The waveguide shown in Fig. 5 is near temperature independent over the entire measured wavelength range (1540-1570 nm), with a residual dn_{eff}/dT from 0 to -1.5×10^{-5} K⁻¹ (dn/dT ~0 at $\lambda = 1540$ nm).

From our SEM measurements, the fabricated waveguide in Fig. 5 was found to be slightly wider compared to the nominal design, due to a 40 nm waveguide width fabrication bias. The measured value of the SU-8 polymer TO coefficient was closer to $-1.3 \times 10^{-4} \text{ K}^{-1}$. We carried out additional simulations with the actual waveguide dimensions as measured by SEM in order to accurately compare the experimental results with the theoretical calculations.

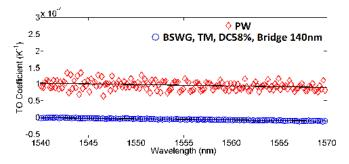


Fig. 5. The thermo-optic coefficient dependence on the wavelength. The TO coefficient of athermal BSWG waveguides are compared with the PW waveguide. The BSWG waveguides were designed nominally athermal at the wavelength $\lambda = 1550$ nm.

The comparison with the experimental results is presented in Fig. 6, where the TO coefficients of BSWG waveguides with 42% and 58% grating duty cycles are shown for TE and TM polarizations as a function of bridge widths. The quoted values for the width and duty cycle of all experimental structures are the actual values as determined by the SEM images. In terms of the fabrication tolerance of the BSWG waveguide, we have found by simulations that the TO effect tolerance due to small changes in the bridge width are not significant. With a 1nm change in bridge width, the TO effect variations are calculated to be approximately $2.6 \times 10^{-7} \text{ K}^{-1}/\text{nm}$ and $7.3 \times 10^{-7} \text{ K}^{-1}/\text{nm}$ for TE and TM polarizations, respectively.

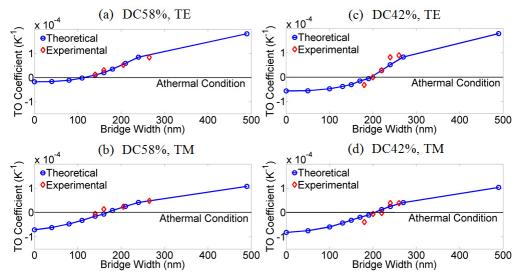


Fig. 6. BSWG thermo-optic coefficient dependence on the bridge width (W₂), for DC = 58% (a, b) and DC = 42% (c, d) for TE and TM polarizations. Simulation results for waveguide dimensions measured by SEM are compared with the experimental data. Waveguide dimensions: W₁ = 490 nm, H = 260 nm, and Λ = 250 nm. The operating wavelength is 1550 nm.

The results in Fig. 6 show that the experiments agree well with the theoretical predictions. Some minor differences are most likely due to uncertainties in the SEM measurement of the actual waveguide dimensions. It should also be noticed that the critical dimensions of the athermal BSWG waveguides demonstrated here are larger than 100 nm and therefore can potentially be fabricated using deep-UV lithography.

4. Conclusion

The temperature-independent bridge subwavelength grating waveguides have been demonstrated for both TE and TM polarizations. Compared to conventional segmented SWG waveguides, the bridging segments provide an extra degree of freedom in the design of the BSWG waveguides, lending to several possible geometries of athermal BSWG waveguides. For a given range of duty cycles, an athermal condition is achieved by a judicious choice of the bridge width, for both TE and TM polarizations. Temperature-independent BSWG waveguides have been demonstrated experimentally for two different duty cycles. Our athermal BSWG waveguides have critical dimensions larger than 100 nm, and can therefore potentially be fabricated by the 193 nm deep-UV lithography. We also showed that athermal operation for both TE and TM polarization is feasible in the same BSWG waveguide, which is an important step towards the development of silicon photonic devices.